Organic Electronics 49 (2017) 400–405

Contents lists available at ScienceDirect

Organic Electronics

journal homepage: www.elsevier.com/locate/orgel

Solution-processable 2,1,3-benzothiadiazole containing compound based on the novel 1-dodecyl-6-dodecoxynaphthyridine-2-one unit for organic field-effect transistors

Joseph Cameron [a], Lana Nanson [b], Nicolas Blouin [b], Neil J. Findlay [a], Anto R. Inigo [a], Peter J. Skabara [a, *]

[a] WestCHEM, Department of Pure and Applied Chemistry, University of Strathclyde, Glasgow, G1 1XL, UK
[b] Merck Chemicals Ltd, Chilworth Technical Centre, University Parkway, Southampton, SO16 7QD, UK

ARTICLE INFO

Article history:
Received 18 May 2017
Received in revised form
16 June 2017
Accepted 3 July 2017
Available online 4 July 2017

Keywords:
Organic field-effect transistor (OFET)
Organic semiconductors
Solution-processing
Novel acceptor unit
Naphthyridine

ABSTRACT

Small molecule organic semiconductors have well-defined structures and can be used in place of polymers which often show batch-to-batch variation. Many different electron-rich donor and electron-deficient acceptor units have been used to design materials with reduced HOMO-LUMO gaps and improved mobilities. Here we introduce a novel acceptor unit, 1-dodecyl-6-dodecoxynaphthyridine-2-one. This acceptor unit has been used in the synthesis of two novel compounds, with thiophene and 2,1,3-benzothiadiazole (BT) cores. The BT-containing compound shows a narrower HOMO-LUMO gap, broad solid-state absorption and has been applied to organic field-effect transistors, showing a mobility of 0.022 $cm^2 V^{-1} s^{-1}$ after optimisation of devices using self-assembled monolayers.

1. Introduction

Organic semiconductors have been successfully applied to organic light-emitting diode (OLED) [1,2], organic photovoltaic (OPV) [3,4] and organic field-effect transistor (OFET) [5,6] technologies and can offer advantages over inorganic-based devices. For example, these materials are flexible, lightweight and can be processed using cheap roll-to-roll fabrication methods such as inkjet printing [7]. Often polymers are used in organic semiconductor devices and, although they can show good performance, polymers often show batch-to-batch variation in molecular weight, polydispersity and physical properties, whilst also displaying end-group variation. These problems can be overcome by using small molecules, which have well-defined monodisperse structures.

Control of the gap between the highest occupied molecular orbital (HOMO) and the lowest unoccupied molecular orbital (LUMO) in small molecules and the band gap in polymers, is important in optimising performance in organic semiconductor devices. A common approach to reducing the HOMO-LUMO (or band) gap is to introduce electron-deficient acceptor units into the conjugated backbone of the organic semiconductor, leading to a reduced LUMO energy (and potentially a lower HOMO energy, but not by the same magnitude). Among the many different acceptor units that have been applied to organic semiconductor devices, nitrogen-containing heterocycles such as diketopyrrolopyrrole (DPP) [8–10], naphthalenediimide (NDI) [11,12], 2,1,3-benzothiadiazole (BT) [13,14] and pyridal[2,1,3]thiadiazole [15,16] have shown high charge carrier mobilities in OFET devices.

The introduction of multiple acceptor units can lead to a much more complex picture. Nguyen et al. [17] have shown that structures containing three DPP units can exhibit higher p-type mobility and OPV power conversion efficiency than analogous compounds containing fewer chromophores due to a low-lying HOMO and improved film morphology. Another interesting example of such compounds are the BODIPY-DPP triads reported by Cortizo-Lacalle et al. [18] where inclusion of BODIPY units significantly alters the absorption, with a broader absorption spectrum and red-shifted DPP absorption band.

Here we report the synthesis of a material based on the 2,1,3-benzothiadiazole acceptor unit containing novel peripheral 1-dodecyl-6-dodecoxynaphthyridine-2-one moieties. Additionally,

* Corresponding author.
E-mail address: peter.skabara@strath.ac.uk (P.J. Skabara).

http://dx.doi.org/10.1016/j.orgel.2017.07.003

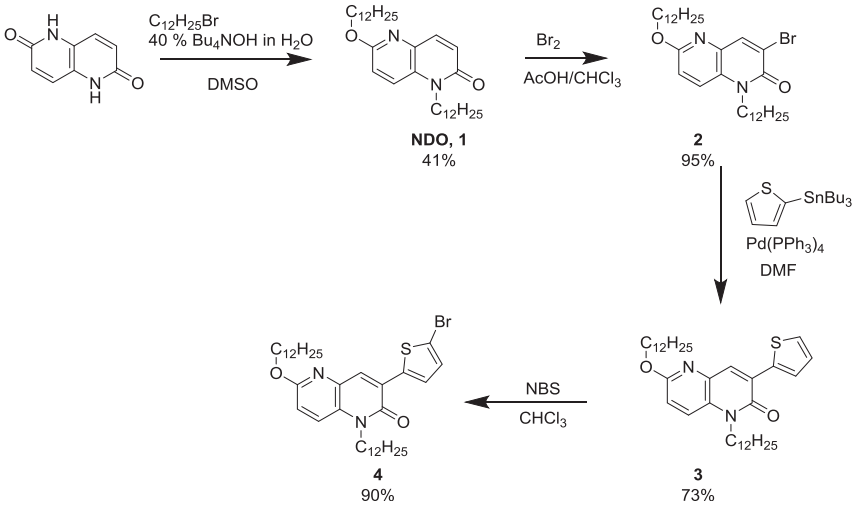

Scheme 1. Synthesis of compounds **1**–**4**.

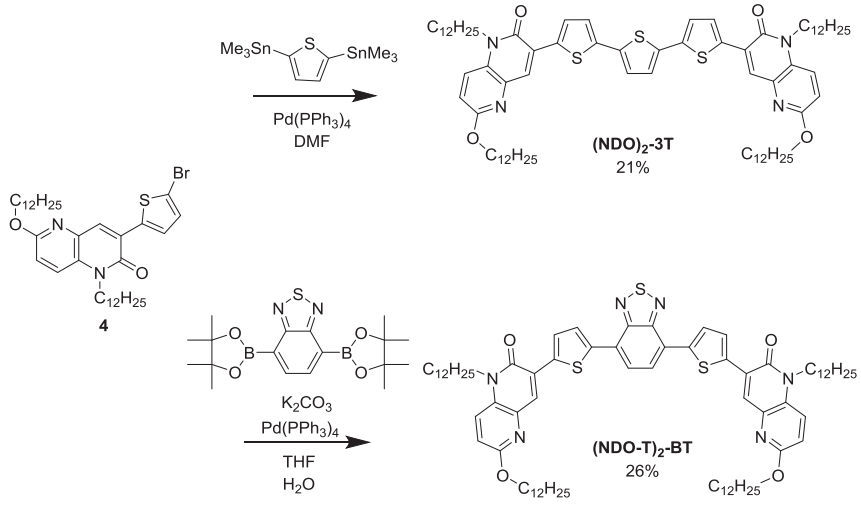

Scheme 2. Synthesis of target molecules **(NDO)$_2$-3T** and **(NDO-T)$_2$-BT**.

an analogous compound was synthesised with a thiophene central unit in place of the electron-deficient BT. The physical properties of the novel compounds are characterised by UV/Vis spectroscopy and cyclic voltammetry (CV), while the effect of incorporating an additional acceptor unit into the conjugated backbone is discussed. Finally, bottom-gate, bottom-contact OFET devices using the BT-containing compound are discussed, along with the effect of self-assembled monolayers (SAMs) and the solvents used for deposition on the performance of the devices.

2. Results and discussion

2.1. Synthesis

The synthetic pathway for the synthesis of the target materials is shown below in Schemes 1 and 2. The first step in the synthesis of the target materials was the alkylation of naphthyridine-2,6-dione, a compound which was synthesised according to previously reported methods [19]. Three isomeric products are formed as a result of this reaction (Fig. 1) but these compounds were separated *via* column chromatography in yields of 41%, 12% and 28% for NDO, NDD and ND respectively.

Bromination of **NDO** (**1**) was performed using bromine, exclusively yielding the mono-brominated product compound **2**, which was subsequently coupled to 2-tributylstannylthiophene *via* Stille coupling to form compound **3**, followed by bromination using *N*-bromosuccinimide (NBS). Compound **4** was used in a Suzuki cross-coupling reaction with 2,1,3-benzothiadiazole-4,7-bis(boronic acid pinacol ester) in order to form **(NDO-T)$_2$-BT** and a Stille coupling reaction with 2,5-bis(trimethylstannyl)thiophene to form **(NDO)$_2$-3T**. The selective bromination of compounds **1** and **3** highlights that **NDO** has the potential to be easily used as a peripheral acceptor unit in combination with a multitude of electron-rich or electron-deficient cores.

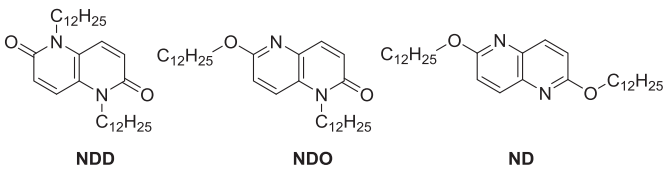

Fig. 1. Isomeric products from alkylation of naphthyridine-2,6-dione.

Table 1
Summary of optical and electrochemical properties of **$(NDO)_2$-3T** and **$(NDO\text{-}T)_2$-BT**.

Compound	$\lambda_{abs\ max}$ (nm)[a]	$\lambda_{em\ max}$ (nm)	E_g^{opt} (eV)[a,b]	E_g^{EChem} (eV)[c]	HOMO (eV)[d]	LUMO (eV)[d]	E_{ox} (V)[e]	E_{red} (V)[e]
$(NDO)_2$-3T	477 (562)	536	2.30 (2.02)	2.03	−5.35	−3.33	0.51, ir	−1.50/-1.28, qr −2.09/-1.78
$(NDO\text{-}T)_2$-BT	516 (649)	609	2.09 (1.76)	1.86	−5.31	−3.45	0.51/0.35, qr 0.93/0.77	−1.36, ir −1.65/-1.56, qr −1.94/-1.84

[a] Solution-state absorption from 10^{-5} M CH_2Cl_2 solutions, solid-state absorption properties shown in parentheses.
[b] Optical HOMO-LUMO gap (Eg) is calculated from the onset of absorption.
[c] Electrochemical HOMO-LUMO gap calculated from the difference between calculated HOMO and LUMO levels.
[d] HOMO (LUMO) level was calculated using the peak of the forward scan of oxidation (reduction) from the following equation: $E^{HOMO(LUMO)} = -4.8\ eV - E_{peak}^{ox(red)}$.
[e] The cathodic and anodic peaks are reported for reversible and quasi-reversible (qr) waves. The peak value on the forward scan is shown for irreversible (ir) waves. The peak values are referenced externally to Fc/Fc^+ (Fig. SI2).

2.2. Optical and electrochemical properties

In order to make a comparison between the two compounds and understand the effect of the incorporation of the BT unit, UV/Vis absorption and fluorescence spectroscopy experiments were carried out in addition to cyclic voltammetry. A summary of these results is listed in Table 1. The absorption spectrum of **$(NDO)_2$-3T**, shown in Fig. 2, reveals a single broad peak with a λ_{max} of 477 nm. However, the absorption spectrum of **$(NDO\text{-}T)_2$-BT** is more complex, indicating a small peak at 423 nm with an associated high energy shoulder, and the main peak at a λ_{max} of 516 nm. This indicates a bathochromic shift, with respect to **$(NDO)_2$-3T**, of 93 nm due to the incorporation of the additional BT unit.

For both molecules the solid-state absorption spectra are broad, with **$(NDO\text{-}T)_2$-BT** in particular absorbing across the visible light region. In general, both absorption profiles are red-shifted in the solid-state compared to solution-state, with the most intense peaks of the absorption spectra of **$(NDO)_2$-3T** and **$(NDO\text{-}T)_2$-BT** being red-shifted by 85 and 133 nm, respectively. There is a significant increase in the red-shift of the most intense absorption peak of **$(NDO\text{-}T)_2$-BT** with respect to **$(NDO)_2$-3T**, due to the reduction in the HOMO-LUMO gap. The solution-state spectrum of **$(NDO)_2$-3T** changes from being broad and featureless to an absorption spectrum showing another peak in addition to a high energy shoulder in the solid-state. This shows evidence of vibronic splitting of **$(NDO)_2$-3T** due to rigidification of the molecules in the film.

There are also considerable differences in the fluorescence spectra of both compounds. The $\lambda_{em\ max}$ for **$(NDO)_2$-3T** was 536 nm, giving a Stokes shift of 59 nm, while the $\lambda_{em\ max}$ of **$(NDO\text{-}T)_2$-BT** was 609 nm, corresponding to a Stokes shift of 97 nm; this is a significant increase with respect to **$(NDO)_2$-3T** showing that the inclusion of the electron-accepting BT unit in the conjugated backbone greatly affects the optical properties of the molecules.

Cyclic voltammetry was also carried out on the novel compounds in order to examine the electrochemical properties and the voltammograms for the oxidation and reduction of **$(NDO)_2$-3T** and **$(NDO\text{-}T)_2$-BT** are shown below in Fig. 3. The oxidation of **$(NDO)_2$-3T** shows one irreversible peak, whilst the BT-containing compound shows a quasi-reversible wave followed by a reversible wave. The first oxidation for each compound occurs at similar potentials, indicating that the common NDO unit is responsible for the first loss of an electron. Considering that this first oxidation peak of **$(NDO)_2$-3T** is irreversible, it seems that the presence of the BT unit may help to stabilise the radical-cation as the first oxidation of **$(NDO\text{-}T)_2$-BT** is quasi-reversible. It can then be assumed that the second oxidation of **$(NDO\text{-}T)_2$-BT** takes place at the BT core, although this occurs at a lower potential than the related 4,7-di(thiophen-2-yl)benzo[c] [1,2,5]thiadiazole (BTB) molecule (Fig. SI1) [20], suggesting that the increased conjugation of **$(NDO\text{-}T)_2$-BT** stabilises the dication.

There are also differences in the reduction of the two compounds. The reduction of **$(NDO)_2$-3T** shows quasi-reversible and reversible waves, respectively, whilst the voltammogram for **$(NDO\text{-}T)_2$-BT** shows an irreversible peak followed by quasi-reversible and reversible waves. The first reduction of **$(NDO\text{-}T)_2$-BT** occurs at a similar potential to BTB [20], suggesting that the reduction takes place at the central BT unit. The reduction of BTB is reversible, however [20], so the presence of the NDO units on **$(NDO\text{-}T)_2$-BT** appears to destabilise the radical anion.

The HOMO and LUMO levels for the two NDO-based compounds are shown in Table 1. The HOMO energy values are similar which is consistent with the oxidation taking place at the NDO unit in both molecules. However, the LUMO energies vary significantly with the LUMO energy of **$(NDO\text{-}T)_2$-BT** calculated to be 0.12 eV lower than

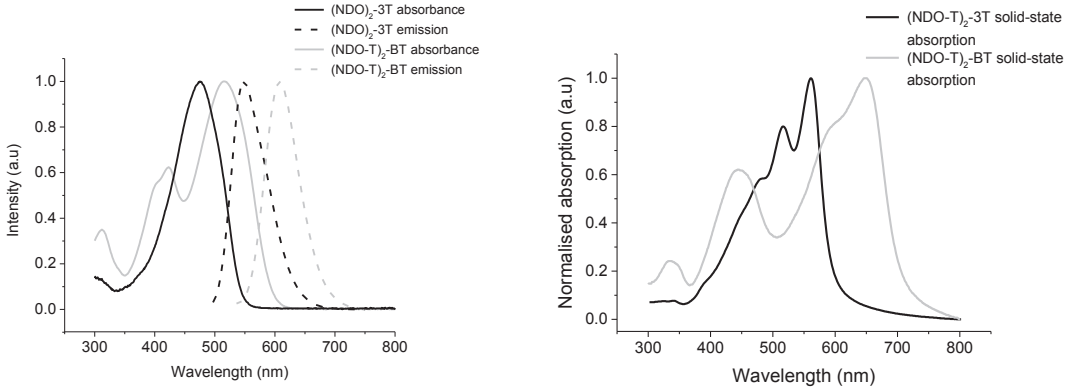

Fig. 2. UV/Vis absorption and emission spectra of 10^{-5} M CH_2Cl_2 solutions of **$(NDO)_2$-3T** and **$(NDO\text{-}T)_2$-BT** (left) and solid-state absorption spectra of **$(NDO)_2$-3T** and **$(NDO\text{-}T)_2$-BT** (right).

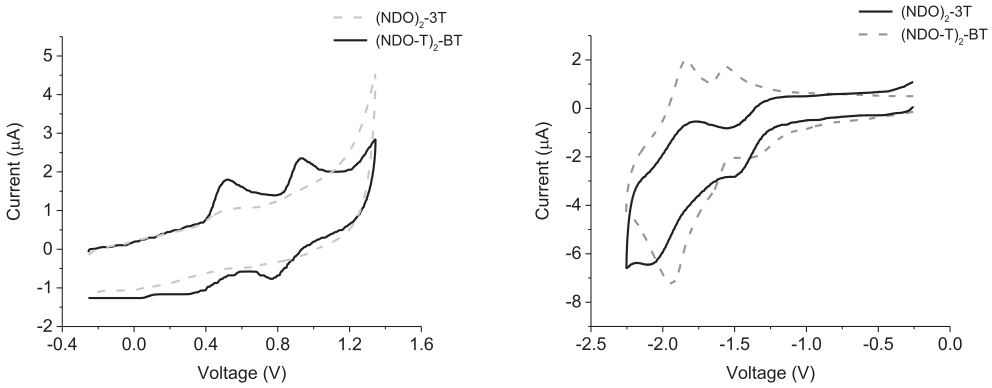

Fig. 3. Oxidation (left) and reduction (right) of **$(NDO)_2$-3T** and **$(NDO\text{-}T)_2$-BT.**

Table 2
OFET results for devices containing films of **$(NDO\text{-}T)_2$-BT** formed from spin-coating $CHCl_3$ solution. Results were calculated from an average of 6 OFET devices.

Self-assembled monolayer	Annealing temperature (°C)	μ_h ($cm^2\ V^{-1}\ s^{-1}$) average	ON/OFF ratio	V_T (V)
PFBT	25	3.6×10^{-3}	10^4	−22
PFBT/OTS	25	2.3×10^{-3}	10^4	−21
OTS	25	0.014	10^4	−28
HMDS	25	5.5×10^{-3}	10^3	−34
PFBT	120	4.6×10^{-3}	10^5	−20
PFBT/OTS	120	4.7×10^{-3}	10^4	−12
OTS	120	0.022	10^4	−16
HMDS	120	3.9×10^{-3}	10^4	−28

that of **$(NDO)_2$-3T**. This suggests that benzothiadiazole is a more dominant acceptor unit than NDO. Substituting the benzothiadiazole unit in place of the central thiophene of **$(NDO)_2$-3T** has little effect on the HOMO level but is an effective means of reducing the LUMO level.

2.3. Organic field-effect transistor (OFET) devices

Bottom-contact bottom-gate OFET devices were fabricated from **$(NDO\text{-}T)_2$-BT** and, in order to optimise the charge carrier mobility, a number of parameters were investigated with respect to the device

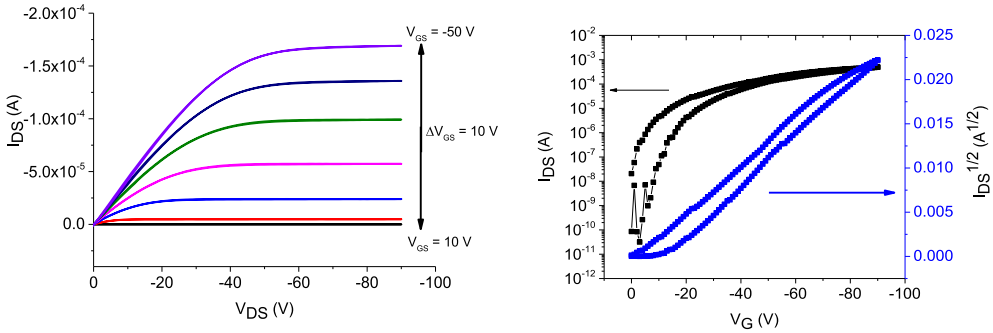

Fig. 4. Output (left) and transfer (V_{DS} = −50 V) (right) graphs of an OFET device containing **$(NDO\text{-}T)_2$-BT**. SAM = OTS; solvent = $CHCl_3$; unannealed. Channel length = 20 μm; channel width = 1 cm.

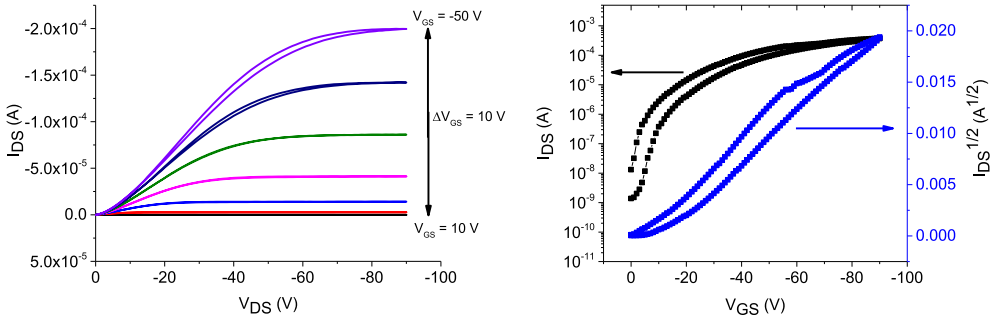

Fig. 5. Output (left) and transfer (V_{DS} = −50 V) (right) graphs of an OFET device containing **$(NDO\text{-}T)_2$-BT**. SAM = OTS; solvent = $CHCl_3$; annealed at 120 °C. Channel length = 5 μm; channel width = 1 cm.

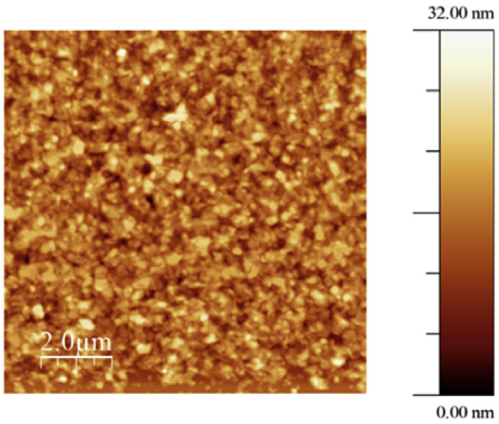

Fig. 6. AFM image of OFET fabricated using OTS SAM and **(NDO-T)$_2$-BT** film cast from $CHCl_3$ solution with annealing at 120 °C. RMS roughness = 3.9 nm.

characteristics. These parameters included the variation of the solvent, self-assembled monolayers (SAMs) and thermal annealing. Chloroform and *o*-dichlorobenzene were studied as the solvents used for spin-coating and pentafluorobenzenethiol (PFBT), octadecyltrichlorosilane (OTS) and hexamethyldisilazane (HMDS) were studied as SAMs. Full experimental details for the fabrication of OFET devices are described in the supplementary information section. **(NDO)$_2$-3T** was not studied due to concerns over the irreversible oxidation of this compound and how this would impact its function as a p-type material in OFETs.

Results for devices fabricated using *o*-dichlorobenzene are summarised in Table SI1 with output and transfer graphs for annealed films shown in Figs. SI3 and SI4. The mobility for unannealed devices with a PFBT SAM is 4.4×10^{-4} cm^2 V^{-1} s^{-1}, although this is improved to 3.3×10^{-3} cm^2 V^{-1} s^{-1}, by annealing at 120 °C and using both PFBT and OTS SAMs. However, the performance is limited by the poor morphology of films cast in *o*-dichlorobenzene solutions, as shown by AFM in Fig. SI8. Devices fabricated from **(NDO-T)$_2$-BT** chloroform solutions show overall higher hole mobilities than those spin-coated from *o*-dichlorobenzene solutions and are summarised in Table 2.

If the optimum conditions for OFETs fabricated using *o*-dichlorobenzene are repeated using chloroform as the solvent then there is an improvement in the hole mobility. Using PFBT (Fig. SI5), PFBT/OTS (Fig. SI7) and HMDS (Fig. SI6) SAMs in the fabrication of OFETs with chloroform as solvent for solution-processing, resulted in hole mobilities of similar magnitude. However, use of OTS as the sole SAM provided a significant increase in hole mobility. The output and transfer graphs for OFETs fabricated with OTS SAM and chloroform **(NDO-T)$_2$-BT** solutions, without annealing and annealed at 120 °C are shown in Figs. 4 and 5, respectively. Without annealing, the average hole mobility is calculated to be $\mu_h = 0.014$ cm^2 V^{-1} s^{-1}; annealing the device at 120 °C gave a further increase to $\mu_h = 0.022$ cm^2 V^{-1} s^{-1}.

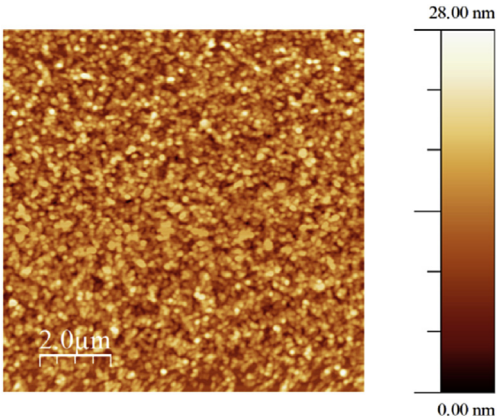

Fig. 7. AFM image of OFET fabricated using OTS SAMs and film cast from $CHCl_3$ solution without annealing. RMS roughness = 3.4 nm.

Analysis of images obtained by AFM shows that, despite there being an order of magnitude difference in the hole mobilities of OFETs fabricated from chloroform with PFBT/OTS and OTS as SAMs, there is little difference in morphology (Fig. SI9 and Fig. 6, respectively). A more homogeneous film due to improved intermolecular stacking interactions may contribute to the increased mobility for the OFET containing only an OTS SAM.

Finally, AFM was used in order to explain the improvement of performance upon annealing. Although there is only a small increase in mobility when the OFET containing the OTS SAM is annealed, there are slight differences in the films to explain this. The surface of the unannealed sample (Fig. 7, Fig. SI10) shows small aggregates that appear to increase in size after annealing (Fig. 6, Fig. SI10). Given that the roughness of these films is similar, the increased area of these aggregates could lead to improved charge transport through the film.

3. Conclusions

Herein, we have presented the synthesis and characterisation of two novel compounds based on the novel, asymmetric heterocyclic acceptor unit 1-dodecyl-5-dodecoxynaphthyridin-2-one. UV/Vis absorption and fluorescence spectroscopy were used to determine the optical properties of the target materials with cyclic voltammetry used to characterise the electrochemical properties. Incorporation of the BT unit into the conjugated backbone (**(NDO-T)$_2$-BT**) showed a broader absorption, particularly in the solid-state, and a larger Stokes-shift with respect to **(NDO)$_2$-3T**. Furthermore, the inclusion of the BT unit significantly lowered the LUMO level, whilst the HOMO energy was similar in both compounds. By varying the central unit it could be possible to easily synthesise NDO-based materials with diverse properties suitable for various different organic electronic applications.

OFET devices were fabricated using **(NDO-T)$_2$-BT** and, through optimisation of the use of SAMs, solvent and thermal annealing, it was possible to improve the p-type mobility by almost two orders of magnitude whilst maintaining a high ON/OFF ratio and low threshold voltage.

Acknowledgements

JC thanks Merck Chemicals and EPSRC for the Industrial Case PhD funding (EP/K502297/1). PJS thanks the Royal Society for a Wolfson Research Merit Award.

Appendix A. Supplementary data

Supplementary data related to this article can be found at http://dx.doi.org/10.1016/j.orgel.2017.07.003.

References

[1] Q. Zhang, B. Li, S. Huang, H. Nomura, H. Tanaka, C. Adachi, Efficient blue organic light-emitting diodes employing thermally activated delayed fluorescence, Nat. Photonics 8 (2014) 326–332, http://dx.doi.org/10.1038/nphoton.2014.12.

[2] A.L. Fisher, K.E. Linton, K.T. Kamtekar, C. Pearson, M.R. Bryce, M.C. Petty, Efficient deep-blue electroluminescence from an ambipolar fluorescent

emitter in a single-active-layer device, Chem. Mater. 23 (2011) 1640–1642, http://dx.doi.org/10.1021/cm103314t.
[3] I.A. Wright, A.L. Kanibolotsky, J. Cameron, T. Tuttle, P.J. Skabara, S.J. Coles, C.T. Howells, S.A.J. Thomson, S. Gambino, I.D.W. Samuel, Oligothiophene cruciform with a Germanium spiro center: a promising material for organic photovoltaics, Angew. Chem. Int. Ed. 51 (2012) 4562–4567, http://dx.doi.org/10.1002/anie.201109074.
[4] Y. Sun, G.C. Welch, W.L. Leong, C.J. Takacs, G.C. Bazan, A.J. Heeger, Solution-processed small-molecule solar cells with 6.7% efficiency, Nat. Mater. 11 (2011) 44–48, http://dx.doi.org/10.1038/nmat3160.
[5] H. Usta, C. Risko, Z.M. Wang, H. Huang, M.K. Deliomeroglu, A. Zhukhovitskiy, A. Facchetti, T.J. Marks, Design, synthesis, and characterization of ladder-type molecules and polymers. Air-stable, solution-processable n-channel and ambipolar semiconductors for thin-film transistors via experiment and theory, J. Am. Chem. Soc. 131 (2009) 5586–5608, http://dx.doi.org/10.1021/ja809555c.
[6] I. Meager, M. Nikolka, B.C. Schroeder, C.B. Nielsen, M. Planells, H. Bronstein, J.W. Rumer, D.I. James, R.S. Ashraf, A. Sadhanala, P. Hayoz, J.C. Flores, H. Sirringhaus, I. McCulloch, Thieno[3,2-b]thiophene flanked isoindigo polymers for high performance ambipolar OFET applications, Adv. Funct. Mater. 24 (2014) 7109–7115, http://dx.doi.org/10.1002/adfm.201402307.
[7] A. Teichler, J. Perelaer, U.S. Schubert, Inkjet printing of organic electronics – comparison of deposition techniques and state-of-the-art developments, J. Mater. Chem. C 1 (2013) 1910, http://dx.doi.org/10.1039/c2tc00255h.
[8] D. Cortizo-Lacalle, S. Arumugam, S.E.T. Elmasly, A.L. Kanibolotsky, N.J. Findlay, A.R. Inigo, P.J. Skabara, Incorporation of fused tetrathiafulvalene units in a DPP-terthiophene copolymer for air stable solution processable organic field effect transistors, J. Mater. Chem. 22 (2012) 11310–11315, http://dx.doi.org/10.1039/c2jm31502e.
[9] E.D. Głowacki, H. Coskun, M.A. Blood-Forsythe, U. Monkowius, L. Leonat, M. Grzybowski, D. Gryko, M.S. White, A. Aspuru-Guzik, N.S. Sariciftci, Hydrogen-bonded diketopyrrolopyrrole (DPP) pigments as organic semiconductors, Org. Electron 15 (2014) 3521–3528, http://dx.doi.org/10.1016/j.orgel.2014.09.038.
[10] Y.N. Li, P. Sonar, L. Murphy, W. Hong, High mobility diketopyrrolopyrrole (DPP)-based organic semiconductor materials for organic thin film transistors and photovoltaics, Energy Environ. Sci. 6 (2013) 1684–1710, http://dx.doi.org/10.1039/c3ee00015j.
[11] M. Sommer, Conjugated polymers based on naphthalene diimide for organic electronics, J. Mater. Chem. C 2 (2014) 3088–3098, http://dx.doi.org/10.1039/C3TC31755B.
[12] L.E. Polander, S.P. Tiwari, L. Pandey, B.M. Seifried, Q. Zhang, S. Barlow, C. Risko, J.L. Brédas, B. Kippelen, S.R. Marder, Solution-processed molecular bis(naphthalene diimide) derivatives with high electron mobility, Chem. Mater. 23 (2011) 3408–3410, http://dx.doi.org/10.1021/cm201729s.
[13] P. Sonar, E.L. Williams, S.P. Singh, S. Manzhos, A. Dodabalapur, A benzothiadiazole end capped donor-acceptor based small molecule for organic electronics, Phys. Chem. Chem. Phys. 15 (2013) 17064–17069, http://dx.doi.org/10.1039/c3cp52929k.
[14] B. Fu, J. Baltazar, Z. Hu, A. Chien, S. Kumar, C.L. Henderson, D.M. Collard, E. Reichmanis, High charge carrier mobility, low band gap donor – acceptor benzothiadiazole-oligothiophene based polymeric semiconductors, Chem. Mater. 24 (2012) 4123–4133, http://dx.doi.org/10.1021/cm3021929.
[15] H.R. Tseng, H. Phan, C. Luo, M. Wang, L.A. Perez, S.N. Patel, L. Ying, E.J. Kramer, T.Q. Nguyen, G.C. Bazan, A.J. Heeger, High-mobility field-effect transistors fabricated with macroscopic aligned semiconducting polymers, Adv. Mater 26 (2014) 2993–2998, http://dx.doi.org/10.1002/adma.201305084.
[16] W. Wen, L. Ying, B.B.Y. Hsu, Y. Zhang, T.-Q. Nguyen, G.C. Bazan, Regioregular pyridyl[2,1,3]thiadiazole-co-indacenodithiophene conjugated polymers, Chem. Commun. 49 (2013) 7192, http://dx.doi.org/10.1039/c3cc43229g.
[17] J. Liu, Y. Sun, P. Moonsin, M. Kuik, C.M. Proctor, J. Lin, B.B. Hsu, V. Promarak, A.J. Heeger, T.Q. Nguyen, Tri-diketopyrrolopyrrole molecular donor materials for high-performance solution-processed bulk heterojunction solar cells, Adv. Mater. 25 (2013) 5898–5903, http://dx.doi.org/10.1002/adma.201302007.
[18] D. Cortizo-Lacalle, C.T. Howells, U.K. Pandey, J. Cameron, N.J. Findlay, A.R. Inigo, T. Tuttle, P.J. Skabara, I.D.W. Samuel, Solution processable diketopyrrolopyrrole (DPP) cored small molecules with BODIPY end groups as novel donors for organic solar cells, Beilstein J. Org. Chem. 10 (2014) 2683–2695, http://dx.doi.org/10.3762/bjoc.10.283.
[19] L. Nanson, N. Blouin, W. Mitchell, S. Tierney, T. Cull, Organic Semiconductors, 2013. WO 2013/182262 A1.
[20] M. Jayakannan, P.A. Van Hal, R.A.J. Janssen, Synthesis and structure-property relationship of new donor-acceptor-type conjugated monomers and polymers on the basis of thiophene and benzothiadiazole, J. Polym. Sci. Part A Polym. Chem. 40 (2002) 251–261, http://dx.doi.org/10.1002/pola.10107.